UV and VUV Ionization of Organic Molecules, Clusters, and Complexes

Markus Marksteiner,*,† Philipp Haslinger,† Michele Sclafani,† Hendrik Ulbricht,†,‡,§ and Markus Arndt†

Faculty of Physics, University of Vienna, Boltzmanngasse 5, A-1090 Vienna, Austria

Received: May 29, 2009; Revised Manuscript Received: July 23, 2009

The generation of organic particle beams is studied in combination with photoionization using UV radiation at 266 nm and vacuum ultraviolet (VUV) light at 157 nm. Single-photon ionization with pulsed VUV light turns out to be sensitive enough to detect various large neutral biomolecular complexes ranging from metal−amino acid complexes to nucleotide clusters and aggregates of polypeptides. Different biomolecular clusters are shown to exhibit rather specific binding characteristics with regard to the various metals that are codesorbed in the source. We also find that the ion signal of gramicidin can be increased by a factor of 15 when the photon energy is increased from 4.66 to 7.9 eV.

Introduction

Photoionization has become a widely used technique for the detection and analysis of neutral molecular beams. For many molecules of biological relevance, the ionization potential lies between 7 and 12 eV. This energy may, for instance, be provided in a multiphoton process,[1−4] which is often implemented using near-resonant two-photon absorption at $\lambda = 250-300$ nm. For various selected molecules, single-photon excitation may also be achieved using vacuum ultraviolet (VUV) laser radiation as generated by excimer lasers,[2,5−7] by synchrotron radiation,[8] or by high harmonic generation of strong infrared lasers.[9]

Photoionization of neutral organic molecules is not only of general interest for analytic mass spectrometry but also for matter wave experiments aiming at either an improved understanding of quantum coherence and decoherence[10−12] or at precise measurements of molecular properties.[13,14]

Several studies over recent decades have indicated that the ionization efficiency is strongly reduced for large molecules.[15,16] In our present experiments, we take up the theme and investigate the formation and ionization of biomolecular complexes in a mass range up to 7500 Da.

Tagging of large molecules with different chromophores has already been demonstrated in earlier experiments.[17,18] We here explore a similar use of aromatic amino acids and nucleotides in some different molecular environments: free and embedded in polypeptides and in large organic clusters.

Organic clusters have attracted increasing interest in their own right. Charged amino acid clusters such as (Ser_n)[19] or metal complexes such as $(Ser_8Na)_n$[20] have been studied with regard to chiral selectivity in gas-phase collisions. Sublimed amino acid cluster ions also led to gas-phase enantioselective substitution reactions between the amino acids.[21]

The interaction with alkali metals may generally result in important configuration changes in DNA, and experiments on the interaction between nucleotides and alkali atoms revealed the preferential coordination of the metals to some nucleotide species.[22] The particular stability of nucleoside quartets as well as the further clustering of these quartets in the presence of alkali atoms has been observed in recent electrospray experiments.[23]

Also, the radiation resistance of nucleotide clusters[24] and the electronic properties of small $AgTrp_n$-clusters[25] shifted into the focus of recent research.

In extension and complement to these earlier studies, we here explore the integration of alkali and alkaline earth metal atoms into neutral amino acid clusters and neutral nucleotide clusters as well as the detection of unusually large aggregates in VUV single-photon ionization.

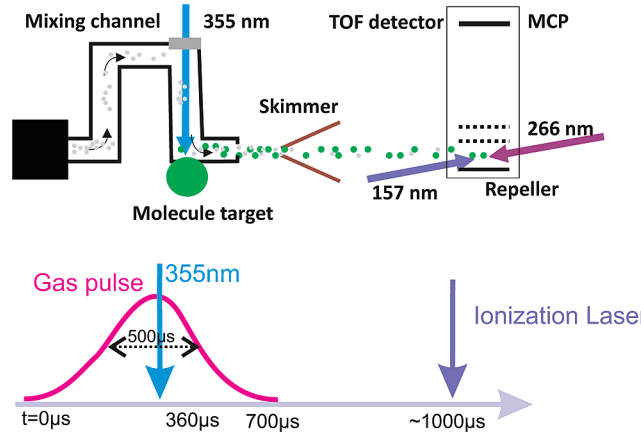

Figure 1. (top) A mixture of biomolecular powder and cellulose is desorbed inside the collision channel. The neutral molecules and clusters propagate through a skimmer toward the time-of-flight mass spectrometer. A quadrupled Nd:YAG laser (266 nm) and a F_2 laser (157 nm) can be alternatively used for the sensitive detection of large organic complexes. (bottom) A time line depicts the crucial steps of the experiment: (1) opening of the valve, (2) desorption shot, and (3) ionization pulse.

Experimental Methods

The general outline of the experiment is similar to our earlier studies[26,27] and is sketched in Figure 1: molecular powder is first admixed with cellulose in a weight ratio of 1:1 to stabilize it against crumbling. It is then pressed onto a threaded metal rod to form the target, which is slowly rotated during the desorption process.

* To whom correspondence should be addressed. E-mail: markus.arndt@univie.ac.at.
† University of Vienna.
‡ University of Southampton.
§ Present address: School of Physics and Astronomy, University of Southhampton, Highfield, Southhampton, SO17 1BJ, United Kingdom.

10.1021/jp905039f CCC: $40.75
Published on Web 08/25/2009

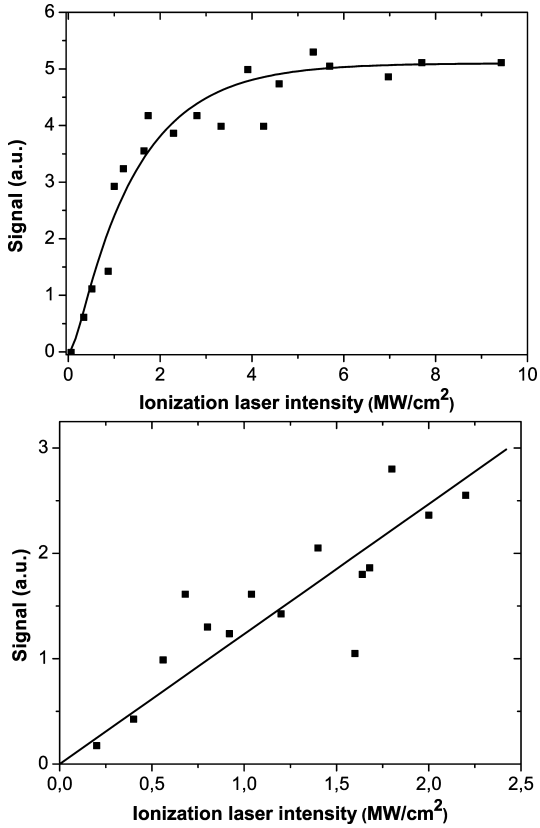

Figure 2. Comparison of the tryptophan ion yield. (top) Ionization with UV (266 nm) light. The saturated curve is fitted by eq 1. (bottom) Ionization with VUV (157 nm) light. The straight line is a guide for the eye.

The molecules are laser desorbed inside a closed mixing channel using a pulsed Nd:YAG laser beam ($\lambda = 355$ nm, $\tau = 5$ ns, $E = 7-10$ mJ). The light beam is focused onto a spot of about 0.5 mm diameter. A fast valve (0.5 mm orifice, 500 μs opening time) injects a noble gas jet with a typical backing pressure of 2 bar into the mixing channel to provide the required cooling and forward acceleration. The pulsed beam of neutral molecules passes a skimmer of 1 mm diameter before it enters the detection chamber (10^{-6} mbar). About 50 cm behind the source, the molecules are photoionized, sorted, and detected in a time-of-flight (TOF) mass spectrometer.

Inside the TOF extraction region, the counter propagating beams of a F_2 excimer laser ($\tau = 5$ ns, $\lambda = 157$ nm) and of a frequency-quadrupled Nd:YAG laser ($\tau = 6-9$ ns, $\lambda = 266$ nm) cross the molecular beam at right angles. Both beams were shaped to have circular profiles with a diameter of 5 mm. The laser energy is measured directly at the laser exit, and we correct for all losses along the optical path. The path of the excimer laser is continuously purged with dry nitrogen to ensure optimal transmission of the VUV radiation. All experiments are performed at a repetition rate of 10 Hz.

Results

UV versus VUV Photoionization of Trp. We start by comparing the photoionization mass spectra of tryptophan (Trp) under irradiation by 266 and 157 nm laser light. While UV ionization at 4.66 eV requires at least a two-photon process, a single VUV photon at 7.9 eV can ionize tryptophan in some conformational states.[28]

We expect to see this difference also in the intensity-dependent ion yield, which is shown in Figure 2. The 266 nm signal increases up to a photon fluence of 5×10^{24} s^{-1} cm^{-2}, that is, a laser intensity of 4 MW/cm^2. The data set is well represented by a saturation curve for a resonant two-photon ionization process:[29]

$$S(I) \propto 1 + \frac{e^{-(s_1+s_2)I\tau/(2h\nu)}(s_1 - s_2)}{2s_2} - \frac{e^{-(s_1-s_2)I\tau/(2h\nu)}(s_1 + s_2)}{2s_2} \quad (1)$$

with $s_1 = 2\sigma_1 + \sigma_2$ and $s_2 = (4\sigma_1^2 + \sigma_2^2)^{1/2}$. Since tryptophan is ionized in a resonant two-step process, σ_1 designates the one-photon cross section for the first transition from the ground state to the intermediate state while σ_2 is the coefficient to lift the electron from the intermediate state into the continuum. The laser intensity is denoted by I, h is Planck's constant, ν is the laser frequency, and τ is the laser pulse duration.

The observation of saturation allows us to extract the absorption cross sections σ_1 and σ_2 even with a rather large uncertainty since the two parameters are not fully independent in eq 1.[29] To fit the tryptophan curve in Figure 2a with eq 1, the data were smoothed and an uncertainty of 20% was taken into account. We thus find the cross sections $\sigma_1 = 1.0(4) \times 10^{-16}$ cm^2 and $\sigma_2 = 6(4) \times 10^{-16}$ cm^2. The systematic uncertainty is estimated to exceed the statistical value by a factor of 2.

The observation of saturation under UV ionization is of practical importance since we can exploit it to generate a stable ion signal: Even though the laser energy of flashlamp pumped lasers may exhibit shot-to-shot fluctuations by 10% or more, its influence on the ion-counting stability is drastically reduced within the saturation plateau.

For single-photon ionization at 157 nm, we expect a linear dependence of the ion yield as a function of the laser power. Figure 2b shows that this is indeed the case. We find no saturation within the available laser intensity, and here we do not need it since the VUV excimer laser (Coherent Existar) is internally energy stabilized to better than 2%. The ion yield is comparable at both wavelengths when the laser intensities are kept on equal levels, that is, when the UV flux is about twice as strong as the VUV flux. On the other hand, laser desorption often causes quite significant fluctuations of the molecular beam intensity. It is not uncommon that signal amplitude variations exceed levels of 50% within a given laser pulse series as shown in Figure 3. This is intolerable in quantitative experiments, and in many cases, we rather require a shot-to-shot stability of better than 10%.

The availability of a second ionization laser pulse can now help us to reduce the source-related signal fluctuations, which may be caused by sample inhomogeneities or fluctuations in the desorption laser intensity. The idea is to derive a normalization signal that varies in proportion to the desired ion count rate.

For that purpose, we use the same molecular desorption pulse twice and send the two ionization laser pulses with a short time delay Δt onto the same molecular cloud. The two pulses interact with two neighboring velocity classes in the molecular beam, but experiments show that the shape of the velocity distribution is rather well reproducible and that the ratio of the two subsequent ionization signals is rather constant even if the molecular beam intensity varies from shot to shot.

The time lag $\Delta t = 12$ μs is chosen to be sufficiently long for the two signals to be separated and stored by the same time-of-flight mass spectrometry (TOF-MS) pulse. It is also suf-

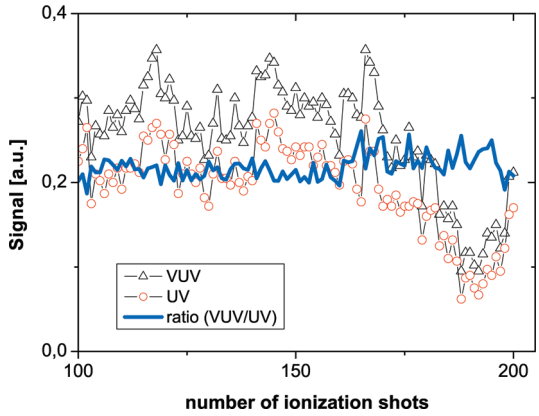

Figure 3. The ionization yield shows strong variations even on a short time scale. A normalization of UV (circles) and VUV (triangles) ionization signals, recorded with only minimal delay, allows us to reduce the source-dependent signal fluctuations by 1 order of magnitude. For clarity, the normalized signal (UV/VUV = solid line) has been scaled by a factor of 6.

ficiently short for both lasers to interact with nearly the same velocity class ($\Delta v/v < 2\%$).

The normalization procedure can be further refined by using different laser beam diameters to interact with different parts of the molecular beam. In our normalization experiments, the VUV laser beam was set to 5 mm whereas the UV beam was vertically focused to below 1 mm.

In Figure 3, we show the raw data of the tryptophan ion signal after VUV and UV excitation. The signals were recorded in two boxcar integrators. The ratio of both curves (VUV/UV) is plotted as the continuous line of Figure 3. While the statistical error of the raw data may even vary by more than 50%, the normalized signal is steadily stabilized to better than 6%. Normalization can thus efficiently eliminate source-related fluctuations by about 1 order of magnitude.

VUV Ionization of Polypeptides and Organic Clusters. The successful ionization of tryptophan with VUV light indicates that this soft detection scheme could be useful also for larger organic molecules and clusters with an ionization energy below 8 eV. Theoretical studies along these lines have been performed by Dehareng and Dive[30] and experiments with Phe-Gly-Gly and beta-carotene have been presented by Wilson et al.[28] We here extend these studies to larger polypeptides as well as to a variety of nucleotide clusters and metal−amino acid complexes.

Gramicidin and Biomolecular Clusters. Gramicidin ionizes well and softly under both UV and VUV irradiation. In both cases, the mass spectrum shows predominantly the pure parent peak centered at 1884 Da and a small forest of peaks below 300 Da but no fragments in-between.

Commercial gramicidin powder consists of a mixture of the four polypeptides gramicidin A, B, C, and D. Their amino acid sequence is HCO-X-Gly-L-Ala-D-Leu-L-Ala-D-Val-L-Val-D-Val-L-Trp-D-Leu-L-Y-D-Leu-L-Trp-D-Leu-L-Trp-$NHCH_2CH_2OH$. Gramicidin A−C differ only by a single amino acid at residue 11 (Y), which can be either tryptophan (A), phenylalanine (B), or tyrosine (C). Gramicidin D is derived from gramicidin A by substituting alanine in place of glycine as the first residue (X). In our powder, the composition was nominally A = 80−85%, B = 6−7%, C = 5−14%, and D < 1% (Sigma Aldrich). All four gramicidin molecules can be detected with both ionization wavelengths (see Figure 4 inset).

Although the mass spectra are rather similar for both excitation wavelengths, the ion yields can differ dramatically as shown in Figure 4. The VUV ion signal of intact gramicidin

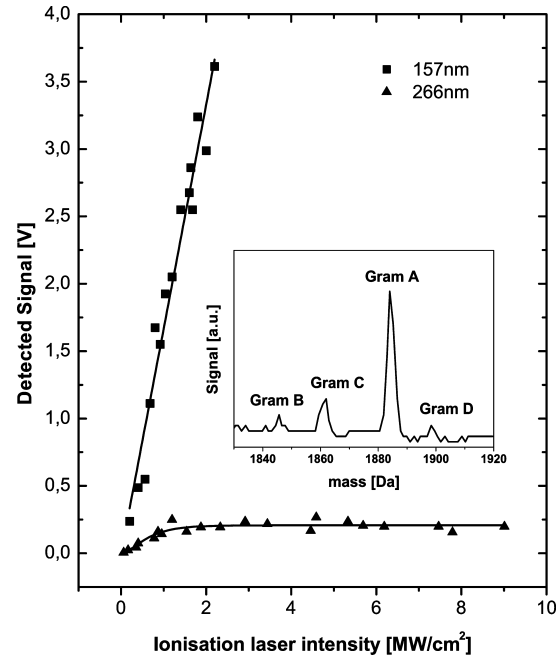

Figure 4. Ion yield of gramicidin A (1884 Da) as a function of the laser intensity at 266 and 157 nm. The 157 nm curve is well-represented by a straight line, whereas the 266 nm curve follows a saturated two-photon ionization curve (eq 1). The inset shows a gramicidin spectrum recorded after UV ionization. All variants from Gram A to Gram D are visible.

A (1884 Da) outperforms the UV ionization already by a factor of 15 at the available VUV laser intensity of 2.2 MW/cm^2. This increase is surprisingly high. The UV absorption spectra of tryptophan and gramicidin in solution[31] are rather similar and suggest that gramicidin actually ionizes via the tryptophan residues that it contains. This argument would rather lead us to expect the ionization yields of gramicidin and tryptophan to have rather the same spectral characteristics. On the other hand, the single-photon ionization efficiency of tryptophan strongly depends on the molecular conformation, and only a small subset of all its possible conformations have a vertical ionization energy that can be accessed by the F_2-laser.[30] Our observation is therefore consistent with the hypothesis that the integration of the tryptophan residues into the polypeptide chain actually favors stabilization of tryptophan conformations with a lower ionization potential.

At 157 nm, the ion yield of gramicidin shows an unsaturated linear increase with the laser intensity. In contrast to that, the 266 nm ionization curve runs again into saturation as also observed for tryptophan. To fit the saturated curve with eq 1, the recorded data were treated as in the case of tryptophan before, and a fit with eq 1 results in $\sigma_1 = 6(2) \times 10^{-16}$ cm^2 and $\sigma_2 = 3(1) \times 10^{-16}$ cm^2. As expected, the gramicidin cross sections are larger than those for tryptophan, but the systematic uncertainties are comparable.

It turns out that VUV ionization is so efficient that also clusters of gramicidin (Gra_n) and mixed amino acid−polypeptide clusters, such as Gra_1Trp_n, can be observed. Figure 5 (top) shows the mass spectrum after the desorption of a gramicidin−cellulose mixture (1:1). Interestingly, only pure gramicidin clusters form. The gramicidin dimer (3768 Da), trimer (5652 Da), and even the neutral tetramer at 7536 Da can still be detected.

During the experiments with pure gramicidin clusters, a linear mixing channel with a 4 mm diameter exit hole was used. For all other runs, we used the meandering desorption tube as shown in the introduction and in Figure 1.

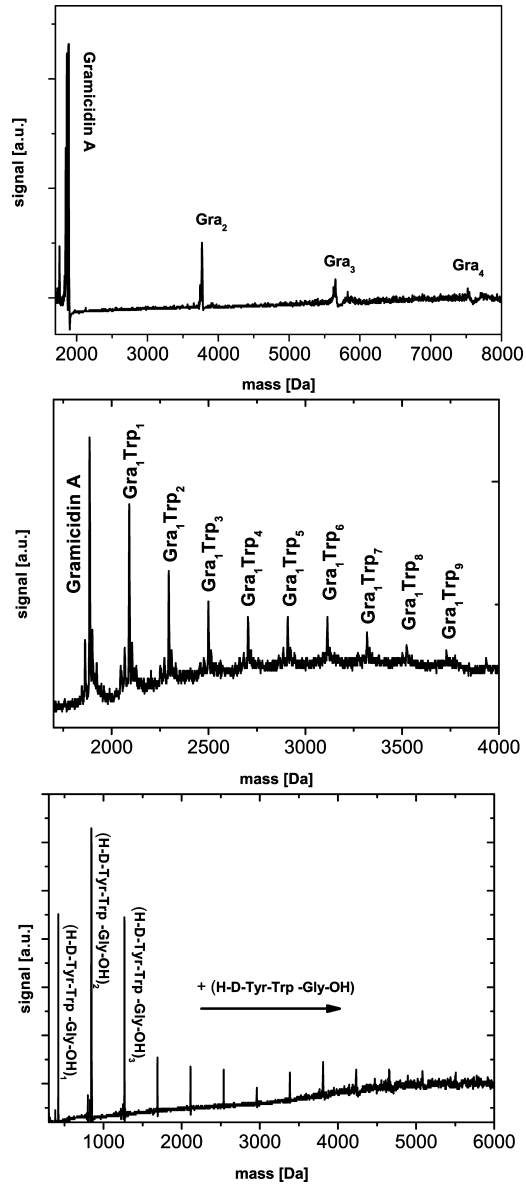

Figure 5. VUV ionization of massive polypeptide clusters. Top: Neutral gramicidin cluster. Center: Tryptophan−gramicidin clusters with admixed insulin. Although insulin was admixed to the same sample, we detect neither any pure insulin nor any trpytophan-tagged insulin under VUV ionization. Bottom: Desorption of H-D-Tyr-Trp-Gly-OH (425 Da) leads to large neutral clusters which can still be detected up to a size of $(H\text{-D-Tyr-Trp-Gly-OH})_{13}$ at a mass of 5500 Da.

Also when using the meandering channel, we find many mixed clusters when we codesorb gramicidin with tryptophan, insulin, and cellulose in a mixture of 0.8:1:1.2:1.6. The mass spectrum is shown in Figure 5 (center). While cluster formation comes not unexpectedly, it is worth noting that Figure 5 (middle) shows only the signal of the gramicidin monomer followed by several peaks which correspond to the sequential addition of single tryptophan molecules. Up to nine tryptophan molecules could be attached to one single gramicidin molecule.

The successful binding between the polypeptide gramicidin and tryptophan as a tag with a low ionization threshold raised hopes that methods such as dye-tagging might also be fruitful for the detection of neutral larger biomolecules, such as insulin. The spectra showed, however, no indication whatsoever of insulin, insulin-tryptophan clusters, or derivatives thereof.

Complementary experiments with the tripeptide H-D-Tyr-Trp-Gly-OH (425 Da, Bachem Inc.) confirmed that also these

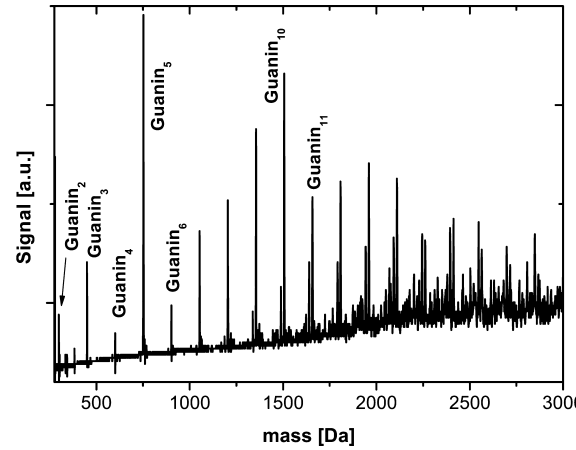

Figure 6. Guanine clusters form during laser desorption into an argon seed gas and are ionized by VUV light. The pentamer G_5 clearly dominates the spectrum. The absence of Ca-complexes is conspicuous in particular in comparison to the amino acid experiments reported below where the integration of a single calcium atom is strongly favored.

particles form large clusters. The tripeptide was desorbed from a highly diluted mixture with the metal salt $CaCO_3$ and cellulose (1:40:100). However, postionization with VUV light revealed a cluster distribution leading up to $(H\text{-D-Tyr-Trp-Gly-OH})_{13}$ as shown in Figure 5 (bottom). In spite of the enormous relative abundance of calcium and cellulose in the sample, the tripeptide clusters always remain pure. This is in marked difference to tryptophan complexes which readily embed a single calcium atom.[26]

The abundance distribution of the tripeptide is nonmonotonic, but we can postionize and detect clusters up to about 6000 Da. This is comparable in size to insulin which remained undetected in all our experiments.

One may ask how the clustering characteristics change if we replace the amino acids by nucleotides. This question has been addressed using a mixture of guanine (151 Da), $CaCO_3$, and cellulose (mixture: 1:1:0.7). The result is shown in Figure 6. The total intensity of all guanine clusters varies from shot to shot, but G_5 always stands out as a particularly abundant, "magic", cluster. It is still an open question whether this phenomenon is related to the particular stability of G_5 or to a favorable tuning of the ionization energies in this particular cluster. The influence of photoinduced fragmentation processes seems to be rather small as the photon energy already matches the ionization threshold[32] and there is hardly any excess energy deposited in the clusters. The observation of the magic G_5 therefore cannot be explained by fragmention during the ionization process.

Magic clusters were also found by others in electrospray ionization experiments with guanine and other nucleotides starting, however, from ions in electrospray experiments.[22] Furthermore, we never observe the inclusion of either calcium or carbonates or cellulose fragments in this series. In case of the guanine, we also repeated the experiment without any metal salts in the sample. We find the same cluster distribution as before. In spite of their abundance, the metal atoms obviously play no role in the formation of the guanine clusters. The role of the metal salts in catalyzing large biomolecular complexes is also discussed in the following section.

Amino Acid−Metal Complexes. The detection of gramicidin and the tripeptide clusters is rather efficient, but photoionization of single large molecules beyond 2000 Da seems generally to

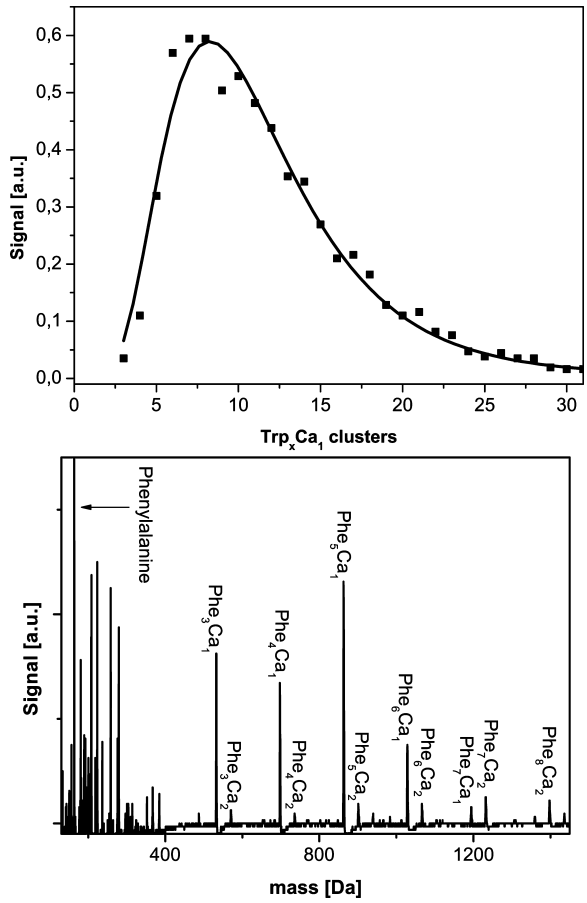

Figure 7. Neutral metal−organic complexes form after laser desorption from a mixture of amino acid powder with a metal salt and cellulose. Top: Cluster distribution of Trp_xCa_1 resulting from desorbed tryptophan and $CaCO_3$ fitted with a log-normal distribution. Ionization of the clusters was done with VUV light, and argon was used as seed gas.[26] Bottom: Phenylalanine and $CaCO_3$ ionized with UV radiation (backing gas: argon).

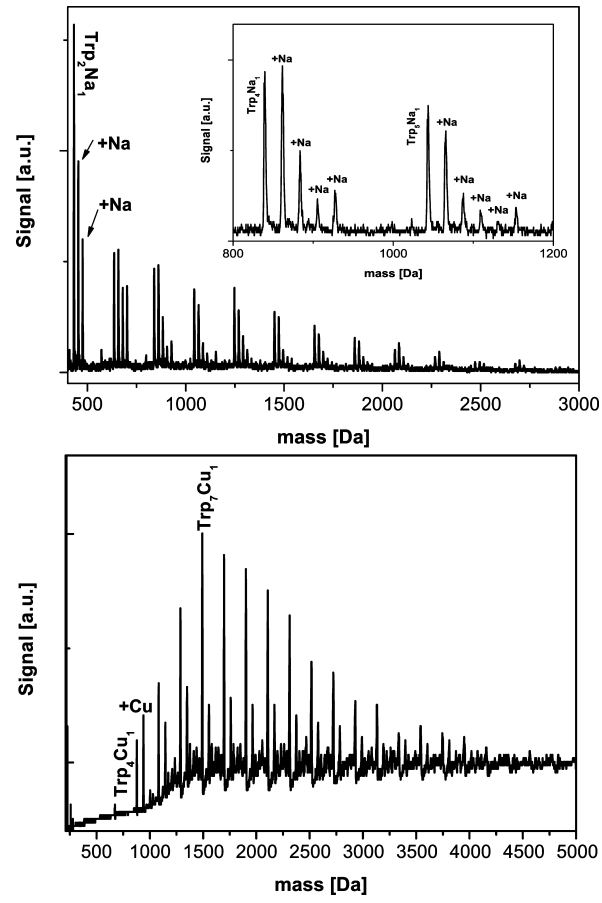

Figure 8. Neutral metal−organic complexes forming after laser desorption from a mixture of the biomolecular powder, the metal salt, and the cellulose. The complexes were ionized using VUV light. (a) Tryptophan and Na_2CO_3 (backing gas: neon). (b) Tryptophan and $CuCO_3$ (backing gas: argon).

be a great challenge. It has been shown in the previous section that the formation and postionization of biomolecular clusters is possible up to a mass of 7500 Da (see Figure 5 top). Also, the presence of alkali earth salts can assist in the formation of large tryptophan clusters, such as Trp_nCa_1 complexes,[26] which could still be photodetected beyond a mass of 6000 Da (Figure 7 top).

It is natural to ask if metal-catalyzed cluster formation also applies to other amino acids, such as phenylalanine (Phe) which shares its aromatic character with tryptophan. The analogy between the two molecules does not, however, extend so far as to allow detection using the same laser frequency. VUV excitation does not result in any measurable Phe ion signal either for the monomer or for any higher cluster.

The ionization energy of phenylalanine was determined to be 8.6 eV[28] and exceeds the energy of a single photon at 157 nm. A VUV two-photon process is not impossible, but it would deposit extra internal energy and fragmentation would become more likely.[33] Accordingly, isolated molecules with an ionization potential exceeding 8 eV, such as phenylalanine or histidine, were never observed in our setup under VUV excitation, whereas they readily appeared after 266 nm two-photon ionization.

Figure 7 (bottom) shows the mass spectrum of phenylalanine that was first desorbed from a balanced mixture of Phe, $CaCO_3$, and cellulose (ratio 1:1:1) and then was ionized at 266 nm. We see the single Phe molecule at 165 Da as well as Phe complexes that contain preferentially one and less frequently two calcium atoms. In contrast to the nucleotide guanine which does not incorporate any metal atom at all, even in the overabundant presence of $CaCO_3$, the amino acid phenylalanine prefers to incorporate a singe metal atom independent of its actual cluster size. This is in agreement with earlier studies of Trp_nCa_1 complexes.[26]

We finally pose the question of how the substitution of alkaline earth salts by alkali or copper salts will influence the amino acid complex formation. Figure 8 (top) shows the mass spectrum after codesorption of tryptophan, Na_2CO_3, and cellulose (mixture: 1:0.3:1.6). We observe dominantly complexes of the form $Trp_nNa_1...Trp_nNa_{n+1}$ as shown in Figure 8 (top). This rule is valid at least up to Trp_5Na_6 and is only violated by the absence of Trp_5Na_5. In the given mass range, the signals are clearly not yet limited by the signal-to-noise ratio or by the availability of metal atoms in the plume. We therefore conclude that the maximum number of metal atoms per cluster is rather determined by the nature of the bonds. A better understanding of the observed cluster rules requires future numerical modeling.

Replacing the metal salt by $CuCO_3$ also leads to the formation of tryptophan−copper clusters as can be seen in Figure 8 (bottom). The cluster formation starts with Trp_4Cu_1, and every Trp_xCu_n cluster can contain one or two copper atoms ($n = 1$, 2). With the exception of Trp_4Cu_1, the signal for Trp_nCu_1 is always stronger than for Trp_nCu_2.

Our experiments showed that the production and detection of metal−biomolecular complexes can be very efficient. In case

of tryptophan, this led again to complexes up to 6000 Da which were generated and detected more readily than clusters without metal inclusions.

When assessing the cluster spectra, one should, however, also bear in mind that we never see the neutral clusters directly but only after postionization in a single-photon process. The incorporation of metal atoms can generally enhance the optical absorption cross section as has recently been shown for small tryptophan−silver complexes.[25]

The abundance distribution of metal−biomolecule clusters is therefore also influenced by modifications of the absorption cross sections and the ionization cross sections.

The metal atoms may also contribute to the cluster stability or to the cluster aggregation time. Generally, they might do this catalytically, that is, without being finally included, or as part of the resulting complex.

Conclusions

The cluster physics or metal−organic system is a rich field. It can be accessed using laser desorption of neutral samples, buffer gas assisted aggregation, and UV/VUV photoionization.

In our experiments, we study the formation and detection of neutral massive clusters and metal−organic complexes which are built from amino acids, nucleotides, and polypeptides in combination with alkali and alkali earth metals.

We find in particular that VUV ionization can be very efficient, and it ionizes the polypeptide gramicidin up to 15 times more efficiently than radiation at 266 nm. Gramicidin can thus be observed even up to the neutral tetramer at 7536 Da.

Desorption of a mixture of tryptophan, gramicidin, and insulin shows that gramicidin−tryptophan clusters can be generated and seen even up to Gra_1Trp_9. In contrast to that, dye-tagging of neutral insulin with tryptophan led to no detectable signals: Insulin−tryptophan complexes were never recorded in our machine. This is in marked difference to tripeptide (H-D-Tyr-Trp-Gly-OH) nucleotide clusters which formed easily detectable aggregates up to masses well comparable to that of insulin.

Our experiments show that metal atom−amino acid complexes can be readily produced when metal−carbonates are codesorbed with organic molecules. Calcium, sodium, and copper atoms were shown to be readily embedded into tryptophan complexes, but they seem to be consistently excluded even by large tripeptide complexes (built from aggregations of H-D-Tyr-Trp-Gly-OH) or by guanine clusters.

The cluster abundance distribution shows a rich structure in almost all of the spectra. Further work is still required to understand the observation of magic cluster numbers and to attribute the relative importance of metal inclusions for either cluster stabilization or cluster detection as well as to elucidate the kinetics of formation, the temperature dependence, and the stability of these large complexes. In this context, it is particularly interesting to study the conspicuous differences in cluster catalysis for different biomolecules in the presence of different metal salts.

Our experiments thus raise many questions which will require further experiments and a thorough theoretical treatment of large complexes. The answers to some of the many open questions may eventually also come from matter wave interferometry, which was the starting point of our own efforts in this field. Recent experiments have shown that near-field interferometry has the potential to provide us with precise static[13] or optical polarizabilities[14] or absolute molecular spectra,[34] which in turn may serve as important benchmark values for future molecular cluster models.

Acknowledgment. The authors thank Christoph Dellago and Harald Oberhofer for fruitful discussions. This work has been supported by the Austrian Science Funds FWF within the Wittgenstein program Z149-N16.

References and Notes

(1) Dey, M.; Moritz, F.; Atkinson, G. H.; Grotemeyer, J.; Schlag, E. *J. Chem. Phys.* **1991**, *95*, 4584–4588.
(2) Köster, C.; Grotemeyer, J. *Org. Mass Spectrom.* **1992**, *27*, 463–471.
(3) Aicher, K. P.; Wilhelm, U.; Grotemeyer, J. *J. Am. Soc. Mass Spectrom.* **1995**, *6*, 1059–1068.
(4) Weinkauf, R.; Schermann, J.-P.; de Vries, M.; Kleinermanns, K. *Eur. Phys. J. D* **2002**, *20*, 309–316.
(5) Arps, J.; Chen, C.; McCann, M.; Datskou, I. *Appl. Spectrosc.* **1989**, *43*, 1211–1214.
(6) Butcher, D. *Microchem. J.* **1999**, *62*, 354–362.
(7) Mühlberger, F.; Wieser, J.; Morozov, A.; Ulrich, A.; Zimmermann, R. *Anal. Chem.* **2005**, *77*, 2218–2226.
(8) Vries, J. D.; Steger, H.; Kamke, B.; Kamke, W.; Drewello, T. *Chem. Phys. Lett.* **1992**, *194*, 452.
(9) Shi, Y. J.; Consta, S.; Das, A. K.; Mallik, B.; Lacey, D.; Lipson, R. H. *J. Chem. Phys.* **2002**, *116*, 6990–6999.
(10) Arndt, M.; Nairz, O.; Voss-Andreae, J.; Keller, C.; der Zouwand, A.; Zeilinger, G. V. *Nature* **1999**, *401*, 680–682.
(11) Gerlich, S.; Hackermuller, L.; Hornberger, K.; Stibor, A.; Ulbricht, H.; Gring, M.; Goldfarb, F.; Savas, T.; Müri, M.; Mayor, M.; Arndt, M. *Nat. Phys.* **2007**, *3*, 711–715.
(12) Hackermüller, L.; Hornberger, K.; Brezger, B.; Zeilinger, A.; Arndt, M. *Nature* **2004**, *427*, 711–714.
(13) Berninger, M.; Stefanov, A.; Deachapunya, S.; Arndt, M. *Phys. Rev. A* **2007**, *76*, 013607−1013607−4.
(14) Gerlich, S.; Gring, M.; Ulbricht, H.; Tüxen, K. H. J.; Mayor, M.; Arndt, M. *Angew. Chem., Int. Ed.* **2008**, *47*, 6195–6198.
(15) Schlag, E. W.; Grotemeyer, J. *Chem. Phys. Lett.* **1992**, *190*, 521–527.
(16) Becker, C. H.; Wu, K. J. *J. Am. Soc. Mass Spectrom.* **1995**, *6*, 883–888.
(17) Hanley, L.; Edirisinghe, P.; Calaway, W.; Veryovkin, I.; Pellin, M.; Moore, J. *Appl. Surf. Sci.* **2006**, *252*, 6723–6726.
(18) Edirisinghe, P. D.; Moore, J. F.; Calaway, I. V.; Wallis, F.; Veryovkin, I.; Pellin, M. J.; Hanley, L. *Anal. Chem.* **2006**, *78*, 5876–5883.
(19) Myung, S.; Julian, R. R.; Nanita, S. C.; Cooks, R. G.; Clemmer, D. E. *J. Phys. Chem. B* **2004**, *108*, 6105–6111.
(20) Takats, Z.; Nanita, S. C.; Cooks, R. G.; Schlosser, G.; Vekey, K. *Anal. Chem.* **2003**, *75*, 1514–1523.
(21) Yang, P.; Xu, R.; Nanita, S. C.; Cooks, R. G. *J. Am. Chem. Soc.* **2006**, *128*, 17074–17086.
(22) Koch, K. J.; Aggerholm, T.; Nanita, S. C.; Cooks, R. G. *J. Mass Spectrom.* **2002**, *37*, 676–686.
(23) Aggerholm, T.; Nanita, S. C.; Koch, K. J.; Cooks, R. G. *J. Mass Spectrom.* **2003**, *38*, 87–97.
(24) Schlathölter, T.; Alvarado, F.; Bari, S.; Lecointre, A.; Hoekstra, R.; Bernigaud, V.; Manil, B.; Rangama, J.; Huber, B. *ChemPhysChem* **2006**, *7*, 2339–2345.
(25) Compagnon, I.; Tabarin, T.; Antoine, R.; Broyer, M.; Dugour, P.; Mitric, R.; Petersen, J.; Bonacic-Koutecky, V. *J. Chem. Phys.* **2006**, *125*, 164326.
(26) Marksteiner, M.; Haslinger, P.; Ulbricht, H.; Sclafani, M.; Oberhofer, H.; Dellago, C.; Arndt, M. *J. Am. Soc. Mass Spectrom.* **2008**, *19*, 1021–1026.
(27) Marksteiner, M.; Kiesewetter, G.; Hackermüller, L.; Ulbricht, H.; Arndt, M. *Acta Phys. Hung. B* **2006**, *26*, 87–94.
(28) Wilson, K. R.; Jimenez-Cruz, M.; Nicolas, C.; Belau, L.; Leone, S.; Ahmed, M. *J. Phys. Chem. A* **2006**, *110*, 2106–2113.
(29) Witzel, B.; Uiterwaal, C. J. G. J.; Schröder, H.; Charalambidis, D.; Kompa, K.-L. *Phys. Rev. A* **1998**, *58*, 3836–3848.
(30) Dehareng, D.; Dive, G. *Int. J. Mol. Sci.* **2004**, *5*, 301–332.
(31) Gotsche, N.; Ulbricht, H.; Arndt, M. *Lasers Phys.* **2007**, *17*, 583–589.
(32) Zavilopulo, A. N.; Shpenik, O. B.; Agafonova, A. S. *J. Phys. B* **2009**, *42*, 025101.
(33) Plekan, O.; Feyer, V.; Richter, R.; Coreno, M.; Prince, K. C. *Mol. Phys.* **2008**, *106*, 1143–1153.
(34) Nimmrichter, S.; Hornberger, K.; Ulbricht, H.; Arndt, M. *Phys. Rev. A* **2008**, *78*, 063607.

JP905039F